Available online at www.sciencedirect.com

SciVerse ScienceDirect

Ceramics International 38 (2012) 1557–1562

CERAMICS INTERNATIONAL

www.elsevier.com/locate/ceramint

Electrochemical characterization of gradient $Sm_{0.5}Sr_{0.5}CoO_{3-\delta}$ cathodes on $Ce_{0.8}Sm_{0.2}O_{1.9}$ electrolytes for solid oxide fuel cells

Chien-Hung Li [a], Shao-Hua Hu [b], Kok-Wan Tay [c], Yen-Pei Fu [a,*]

[a] Department of Materials Science and Engineering, National Dong Hwa University Shou-Feng, Hualien 97401, Taiwan
[b] Department of Environmental Resources Management, Dahan Institute of Technology, Sincheng, Hualien 971, Taiwan
[c] Department of Electronic Engineering, Wu-Feng University, Minhsiung, Chiayi 621, Taiwan

Received 9 June 2011; received in revised form 19 September 2011; accepted 20 September 2011
Available online 28 September 2011

Abstract

This study investigates $Sm_{0.5}Sr_{0.5}CoO_{3-\delta}$ (SSC)–$Ce_{0.8}Sm_{0.2}O_{1.9}$ (SDC) composite cathodes with a gradual change in composition from electrolyte to the cathode in an attempt to discover a potential approach applicable to solid oxide fuel cells (SOFCs). The gradual change in composition from electrolyte to cathode shows the decline in charge transfer resistance (R_2) and gas phase diffusion resistance (R_3). Because the value of R_3 is always larger than R_2 and R_3 significantly dominates the total cathode polarization resistance (R_P) at temperatures within the range of 750–850 °C, i.e., in this temperature range, the rate-determining step is dominated by the diffusion or dissociative adsorption of oxygen. The functionally gradient cathode with a graded interface between cathode and electrolyte reveals both a higher exchange current density (i_0) and a lower activation energy for oxygen reduction reaction (ORR), which suggests that the ORR kinetics can be improved by using the configuration of a functionally gradient cathode.

Keywords: A. Powder: solid state reaction; C. Impedance; D. Perovskites; E. Electrodes; E. Fuel cells

1. Introduction

Recently, solid oxide fuel cells (SOFCs) have attracted a great deal of attention due to the advantages of high electrical efficiency, fuel versatility, low-pollutant emission, etc. [1–3]. However, their high operating temperatures limit the application of SOFCs [4]. Moreover, a lower operating temperature is required. Cathodes are important components of SOFCs, and developing new cathodes which perform well at the intermediate temperatures (600–800 °C) is therefore a key step in reducing operating temperatures. Hence, the conventional SOFCs cathode, strontium doped lanthanum manganite (LSM), is not suitable for intermediate temperature SOFCs due to its low activity below 800 °C [5]. In recent years, potential cathode candidates have normally been based on mixed oxygen ionic and electronic conducting oxides, which have both high ionic and electronic conductivity, and have attracted a lot of attention in terms of their applications for fuel cell electrodes, oxygen separator membranes and membrane reactors for the partial oxidation of methane to syngas [6–8]. The mixed conductivity extends the active oxygen reduction sites from the typical electrolyte–electrode–gas triple-phase boundary to the entire cathode surface, therefore greatly reducing the cathode polarization at low operating temperatures [9]. In particular, rare earth-doped cobaltite has attracted much attention due to its mixed-conduction characteristics and its relatively high ionic conductivity. Strontium-doped samarium cobalite ($Sm_{0.5}Sr_{0.5}CoO_3$) shows high conductivity, up to 10^3 S cm^{-1} [10]. Therefore, $Sm_{0.5}Sr_{0.5}CoO_3$ was selected as the cathode material for investigation in this study. Total cathode polarization resistance includes the effective interfacial polarization resistance corresponding to the electrochemical reactions at the electrode–electrolyte interface and concentration polarization (mass-transfer or gas diffusion polarization) resistance for SOFCs.

In this study, functionally gradient cathodes were used to reduce the cathode polarization resulting from the incompatibility between the cathode and electrolyte. Traditionally, cathodes adjoin the electrolyte in SOFCs, however such dissimilar materials are usually incompatible [11–14]. Abrupt

* Corresponding author. Tel.: +886 3 863 4209; fax: +886 3 863 4200.
E-mail address: d887503@alumni.nthu.edu.tw (Y.-P. Fu).

0272-8842/$36.00
doi:10.1016/j.ceramint.2011.09.041

changes occur in composition and/or microstructure between the cathode and electrolyte. The functionally gradient materials have a gradient interface in which the compositions change gradually from one material to the other [15,16]. The novelty of this study is in its application of the functionally gradient materials concept to the $Sm_{0.5}Sr_{0.5}CoO_{3-\delta}$ cathode. That is, this study investigated the electrochemical properties of gradient a $Sm_{0.5}Sr_{0.5}CoO_{3-\delta}$ (SSC)–$Ce_{0.8}Sm_{0.2}O_{1.9}$ (SDC) composite cathodes on a SDC electrolyte.

2. Experimental

2.1. Cathode and electrolyte materials preparation

2.1.1. $Sm_{0.5}Sr_{0.5}CoO_{3-\delta}$ cathode preparation

The $Sm_{0.5}Sr_{0.5}CoO_{3-\delta}$ (SSC) cathode powder was prepared via the solid-state reaction. Sm_2O_3, $SrCO_3$, and Co_3O_4 powders (>99%) were used as starting materials. These powders were mixed under ethanol and milled for 12 h using zirconia balls. The ball-milled mixture was dried and ground into a powder with mortar and pestle and then calcined in air at 1000 °C for 4 h. The $Sm_{0.5}Sr_{0.5}CoO_{3-\delta}$ powder sample was pelletized with a small amount of PVA as binder with an applied uniaxial pressure of 1000 kgf cm^{-2}. Sintering was carried out in air at a temperature of 1300 °C for 4 h with a programmed heating rate of 5 °C min^{-1}. The sintered samples made up over 95% of the theoretical density in all the specimens.

2.1.2. $Ce_{0.8}Sm_{0.2}O_{1.9}$ electrolyte preparation

The $Ce_{0.8}Sm_{0.2}O_{1.9}$ (SDC) powder was synthesized by coprecipitation using $Ce(NO_3)_3{\cdot}6H_2O$ and $Sm(NO_3)_3{\cdot}6H_2O$ as the starting materials. These starting materials with stoichiometric ratio were dissolved in distilled water and then added to a solution of ammonia. The mixture solution was adjusted to a pH value in the range of 9.5–10. The resultant precipitate was filtered in a vacuum, and washed three times with water and ethanol, respectively. Then, the coprecipitation powder was calcined in air at 600 °C for 2 h. The SDC powder sample were pelletized with a small amount of PVA as binder with an applied uniaxial pressure of 1000 kgf cm^{-2} and the dimensions of 15 mm in diameter and 1 mm in thickness. The disc samples were then finally sintered at 1500 °C for 5 h with a programmed heating rate of 5 °C min^{-1} [17].

2.1.3. Symmetrical fuel cell fabrication

The composite working electrode (WE) was prepared by mixing the $Sm_{0.5}Sr_{0.5}CoO_{3-\delta}$ cathode with $Ce_{0.8}Sm_{0.2}O_{1.9}$ (SDC) electrolyte powders using ball milling. The cathode paste consists of cathode powder, solvent, binder, and plasticizer. The cathode paste was applied on both sides of SDC electrolyte discs with circle patterns using the screen-printing method with a diameter of 13 mm and a thickness of 1 mm. On one side, the cathode paste was painted as the working electrode (WE) with a surface area of 0.385 cm^2. The Pt reference electrode (RE) was located about 0.3–0.4 cm away from the WE. Such a distance was chosen to avoid measurement errors due to the misalignment of the working and counter electrodes [18–20]. The Pt counter electrode (CE) was arranged on the other side of the SDC disk. After the cathode material was painted on the electrolyte, it was then sintered at 1000 °C for 4 h in air. The three different configuration cathodes in this study are schematically illustrated in Fig. 1, and the compositions of three cathode samples are summarized in Table 1. For cathode C, the first layer attached on the SDC electrolyte is composed of 50 wt.% SSC + 50 wt.% SDC, the second one is composed of 70 wt.% SSC + 30 wt.% SDC, and the top layer consists of 100 wt.% SSC.

2.2. Electrochemical measurements

The symmetrical testing-cell experiments were carried out over temperatures ranging from 600 to 850 °C at intervals of 50 °C in a furnace under air ($P_{O_2} = 0.21$ atm). Linear sweep voltammetry between −0.3 and 0.1 V with a sweep rate of 0.5 mV s^{-1} versus the RE was performed using the VoltaLab PGZ301 potentiostat. The frequency applied range of the AC impedance measurements ranged from 100 kHz to 0.1 Hz with 10 mV AC signal amplitude. The EIS fitting analysis was performed with Zview software.

2.3. Materials characterization

The sintered cathodes were characterized by X-ray powder diffractometer (XRD; Rigaku D/MAX-2500V), with a scanning rate of 4° min^{-1} and a scanning range of 15°–75° using a Cu Kα(1.5418 Å) radiation source. The thickness and morphology of the symmetrical testing-cells were measured by scanning electron microscopy (SEM; Hitachi 3500H). The compositions of the SSC–SDC composite cathodes were analyzed by energy dispersive X-ray spectroscopy (EDS).

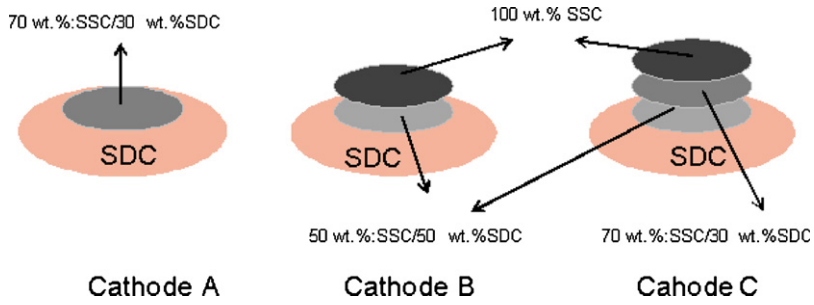

Fig. 1. Schematic diagram of one side of the cathode-half-cell structure for cathode A, cathode B, and cathode C.

Table 1
Summary of three cathode samples.

Sample	Compositions		
	Layer 1	Layer 2	Layer 3
Cathode A	70 wt.% SSC/30 wt.% SDC		
Cathode B	50 wt.% SSC/50 wt.% SDC	100 wt.% SSC	
Cathode C	50 wt.% SSC/50 wt.% SDC	70 wt.% SSC/30 wt.% SDC	100 wt.% SSC

3. Results and discussions

The investigation of the solid-state reactions between SSC and SDC phases is very important for evaluating the cathode polarization resistance of SSC + SDC composite cathodes. Fig. 2 shows the XRD patterns of 50 wt.% SSC + 50 wt.% SDC calcined at various temperatures. Pure SSC contains a perovskite structure, while SDC contains a cubic fluorite-type structure. The results reveal that no obvious interface reaction appeared for SSC + SDC composites when heated up to 1000 °C for 4 h. Xia found that secondary phases were present when $Sm_{0.5}Sr_{0.5}CoO_3$ (SSC) with 10 wt. % SDC composite was calcined at 1250 °C for 4 h [21]. This suggests that a certain degree of solid-state reaction might have occurred between the SSC and SDC phases at 1250 °C. In this study, the SSC + SDC composite was a chemically stable cathode material for SDC electrolyte based SOFCs when the calcined temperature was below 1000 °C. In general, a composite cathode material sintered at a high temperature with a larger grain size leads to a decrease in the electrode surface area–gas solid interface (triple phase boundary, TPB), which results in high polarization resistance [22,23]. Meanwhile, due to the high sintering temperature, the cathode materials adhere strongly to the SDC electrolyte surface, resulting in better contact with the electrolyte and better current collection. This represents a trade-off relationship with regard to the sintering temperature to obtain cathode materials with fine microstructure and strong adhesion to the electrolyte. Fig. 3 shows the interface SDC/50 wt.%SSC + 50 wt.%SDC/70 wt.%SSC + 30 wt.%SDC/SSC of the cathode C and SDC electrolyte sintered at 1000 °C. This figure indicates that the cathode had good adhesion to the electrolyte. No obvious cracks appeared at the interface between the SSC cathode and SDC electrolyte. The EDS data corresponding to the different layers of cathode C are listed in Table 2. The results show that the compositions of different layers agreed with the experimental configuration designed in this study. The element amounts of Sm, Sr, and Co gradually increased from layer 1 to layer 3, whereas the element amount of Ce displayed an inverse tendency.

The cathode performance of SSC-based cathodes was investigated using AC impedance spectroscopy based on a symmetrical testing cell sintered at 1000 °C for 4 h and recorded under open-circuit conditions in air. The polarization resistances of SSC-based cathodes were measured directly from the difference between high- and low-frequency intercepts on the real axis of the impedance plot [24]. Fig. 4 shows the impedance spectra measured under open-circuit conditions in the temperature range of 750–850 °C, in air, for different composite cathodes. In this study, we used an equivalent circuit of the impedance curve as symmetrical testing cells, as shown in Fig. 4. In the present case, in place of a capacitor, a constant phase element (CPE) was applied to model the experimental data. The CPE is equivalent to a distribution of capacitors in parallel. R_1 represents the Ohmic resistance of the cell and R_2 represents the resistance corresponding to the cathode polarization. CPE can be expressed as follows, $Z = 1/C(j\omega)^n$, where C indicates the ideal capacitance ($n = 1$), $j = (-1)^{1/2}$, and ω is the angular frequency and the values of n describe the

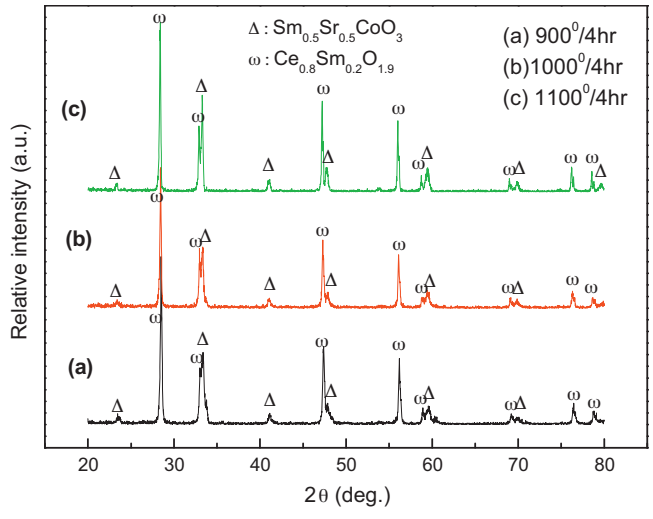

Fig. 2. X-ray diffraction pattern of the powder mixture of 50 wt.% SSC + 50 wt.% SDC calcined at (a) 900 °C, (b) 1000 °C, and (c) 1100 °C for 4 h.

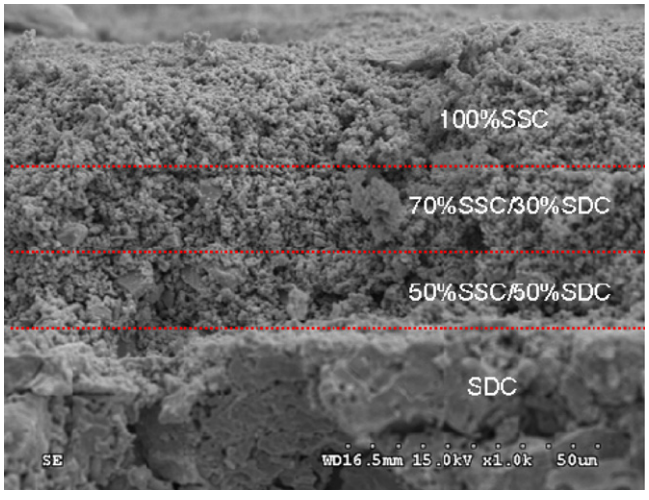

Fig. 3. SEM images of a cross-sectional view of cathode C.

Table 2
The EDS data of Cathode C for layers 1–3.

Layer	Atom (%)				
	Ce K	Co K	Sm L	Sr L	O K
1	13.96	12.03	8.48	7.60	57.93
2	8.41	17.91	9.65	9.17	54.86
3	0.76	20.49	11.04	11.81	55.90

fractal character (i.e. the heterogeneous or porous character) of the sample, the value of which is between 0 and 1 [25]. The high-frequency intercept of the impedance spectrum gives the Ohmic resistance of the cell (R_Ω), including the resistance contributions of the electrolyte, the two electrodes, the current collectors and the lead wires. The low-frequency intercept gives the total resistance (R_T), which is the sum of the Ohmic resistance of the cell (R_Ω) and the total cathode polarization resistance (R_P), including the effective interfacial polarization resistance corresponding to the electrochemical reactions at the electrode–electrolyte interface (R_2) and concentration polarization (i.e. mass-transfer or gas diffusion polarization) resistance (R_3). For the total cathode polarization resistance, the resistance at high frequency is probably associated with charge transfer processes (R_2), which includes the electron-transfer and ion-transfer processes occurring at the current collector/cathode electrode and cathode electrode/electrolyte interfaces, respectively. The low frequency arc can be attributed to the diffusion processes (R_3), which include adsorption–desorption of oxygen, oxygen diffusion at the gas–cathode surface interface, and surface diffusion of intermediate oxygen species [26–29]. In order to clearly show the difference in the cathode polarization behavior, the Ohmic resistance of the cell (R_Ω) was eliminated in the impedance plot. The catalytic activity of the SSC-based cathodes, as characterized by the total cathode polarization resistance (R_P), was determined from the size of the impedance loop. With an increase in the number of cathode layers, there was a significant decrease in the total cathode polarization, implying a decrease in the impedance of O_2 reduction on the SDC electrolyte, i.e., the enhancement of electrochemical activity. The area-specific resistances (ASR) of R_P of cathode A were 0.277, 0.150, and 0.089 Ω cm^2 at 750, 800, and 850 °C, respectively. For cathode B, R_P was reduced to 0.227, 0.120, and 0.075 Ω cm^2 at 750, 800, and 850 °C, respectively. As for cathode C, R_P was further reduced to 0.158, 0.108, and 0.059 Ω cm^2 at 750, 800, and 850 °C, respectively, indicating an approximately 30–40% improvement in terms of electrochemical performance, compared with cathode A. The dramatic decrease in R_P is mainly due to the gradual change in composition from electrolyte to cathode with dissimilar material structure. As shown in Table 3, the value of the gas phase diffusion resistance (R_3) is always noticeably larger than that of the charge transfer resistance (R_2). This implies that R_3 dominates the total cathode polarization resistance (R_P) at temperatures within the range of 750–850 °C. Regardless of their initial values, resistances (R_2 or R_3) gradually reduced from cathode A to cathode C. The reduction in charge transfer resistance (R_2) for cathode C may be related to the fact that the microstructure of the electrode/electrolyte interfaces is obviously improved, whereas the decrease in the gas phase diffusion resistance (R_3) could be ascribed to the increase in the area of triple phase boundaries, which enhanced the surface exchange of oxygen. The excellent performance of cathode C is due to the fact that the optimum interface of SSC/SDC may be achieved by the gradual change in composition from electrolyte to cathode, resulting in the decline in charge transfer resistance (R_2) and gas phase diffusion resistance (R_3). The functionally gradient composite cathode displayed excellent performance in terms of its electrochemical properties. Therefore, this fabrication approach can be applied in the cathode/electrolyte interfaces of SOFCs to obtain excellent cell performance.

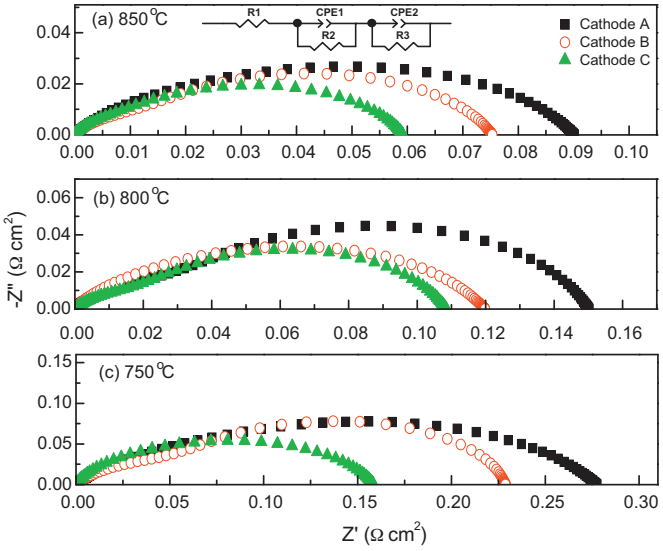

Fig. 4. Nyquist plots and equivalent circuits of EIS for SSC-based cathodes with different temperatures: (a) 850 °C, (b) 800 °C, and (c) 750 °C.

The exchange current density, i_0, which corresponds to the intrinsic oxygen reduction reaction (ORR) rate, is an important parameter for investigating oxygen reduction reaction mechanisms at the cathode [30]. Generally speaking, the oxygen reduction reaction can be divided into several elemental steps:

Table 3
Results of the fitting parameters of SSC-based cathodes measured at different temperatures.

Specimens	750 °C		800 °C		850 °C	
	R_2 (Ω cm^2)	R_3 (Ω cm^2)	R_2 (Ω cm^2)	R_3 (Ω cm^2)	R_2 (Ω cm^2)	R_3 (Ω cm^2)
Cathode A	0.064	0.213	0.034	0.116	0.023	0.066
Cathode B	0.063	0.164	0.032	0.088	0.013	0.062
Cathode C	0.034	0.124	0.022	0.086	0.008	0.051

(1) diffusion of oxygen molecules in the gas phase to the electrode, (2) oxygen dissociate adsorption on the cathode surface, (3) surface diffusion of oxygen on the cathode, (4) incorporation of oxygen into the electrolyte via the triple phase boundary (TPB), and (5) oxide ion diffusion in the bulk of the cathode, and oxide ion transfer from cathode to electrolyte [31,32]. When the exchange current density is higher, the overpotential of the cathode is lower, suggesting that cathodes with high exchange current density value exhibit high performance in terms of electrochemical properties. The i_0 value can be obtained from the AC impedance measurement (EIS). In this technique, i_0 was measured from the polarization resistance, R_P, of the Nyquist plot and calculated using Eq. (1) which is derived from the Bulter–Volmer equation [33]:

$$i_0 = \frac{RT\upsilon}{nFR_P} \quad (1)$$

Here n is the total number of electrons passed in the reaction, υ reflects the number of times the rate-determining step occurs for one occurrence of the full reaction, F is the Faraday constant ($F = 96{,}500$ C mol^{-1}), and R is the ideal gas constant ($R = 8.31$ J mol^{-1} K^{-1}). For the ORR, n andυ are generally assumed to be 4 and 1, respectively (as the total number of electrons transferred per molecule of oxygen reduced is 4 and the rate-limiting step would likely have a stoichiometry of 1 for the oxygen reduction reaction) [34].

The i_0 values for the different cathode-half-cell structures measured from Eq. (1) for EIS are given in Table 4, and their Arrhenius plots for i_0 values as a function of temperature are shown in Fig. 5. The linearity of the Arrhenius plots indicates that the functionally gradient cathodes are stable as a function of temperature. At 800 °C, the i_0 values for cathode B and cathode C determined by the EIS were 192.3 and 235.4 mA cm^{-2}, respectively, both of which were larger than the i_0 value of 160 mA cm^{-2} for LSM/YSZ at the same temperature [34]. From the slope of the line in the Arrhenius plots, the overall activation energy for the ORR was determined by the following equation.

$$\ln i_0 = \ln K - \frac{E_a}{RT} \quad (2)$$

where K is the pre-exponential constant, which can be calculated from the y-intercept, and E_a is the reaction activation energy [35]. The activation energy (E_a) for the ORR may be related to different cathode preparation methods, to the structure of the cathode, or to different cathode compositions. The ORR activation energies obtained from the slope of the Arrhenius plots were 109.5, 108.9, and 105.7 kJ mol^{-1} for cathode A, cathode B, and cathode C, respectively. This suggests that the functionally gradient cathodes with graded interfaces between cathode and electrolyte possess higher exchange current density (i_0) and lower activation energy for the ORR, which indicates that the ORR kinetics can be improved by using the configuration of a functionally gradient cathode.

Table 4
Exchange current density for the SSC-based cathodes using EIS technique in the temperature range of 600–850 °C.

T (°C)	i_0 (mA cm^{-2})		
	Cathode A	Cathode B	Cathode C
600	9.65	11.98	16.22
650	19.31	23.91	33.07
700	41.09	48.90	76.67
750	79.41	96.31	139.03
800	153.48	192.30	235.44
850	268.49	321.26	407.94

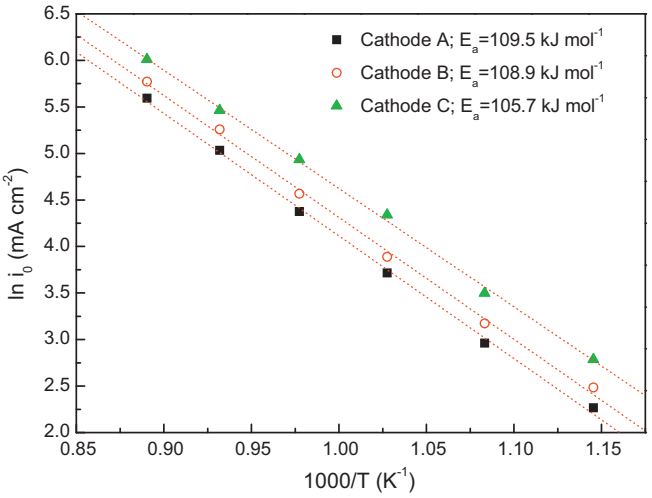

Fig. 5. Arrhenius plots of the exchange current density (i_0) as a function of temperature for different cathode-half-cell configurations.

4. Conclusions

In this study, a $Sm_{0.5}Sr_{0.5}CoO_{3-\delta}$ (SSC)–$Ce_{0.8}Sm_{0.2}O_{1.9}$ (SDC) composite cathodes with a gradual change in composite from electrolyte to cathode was investigated to develop a new approach for solid oxide fuel cells (SOFCs) which reduces the total cathode interface resistance. The results revealed that the total cathode polarization resistance (R_P), charge transfer resistance (R_2) and gas phase diffusion resistance (R_3) were the lowest for a SSC–SDC composite cathodes with three layers and gradient changes in composition from electrolyte to cathode measuring 0.059, 0.008, and 0.051 Ω cm^2, respectively, at 850 °C. SEM images showed that the interface of SSC–SDC composite cathodes with gradual changes in composite between the SSC cathode and SDC electrolyte exhibited good adhesion resulting in the reduction in charge transfer resistance (R_2). This may be related to the microstructure of electrode/electrolyte interfaces. Moreover, the decrease in gas phase diffusion resistance (R_3) may be associated with the area of triple phase boundaries. This implies that the functionally gradient composite cathode showed excellent performance in terms of its electrochemical properties. The functionally gradient cathode with a graded interface between the cathode and electrolyte revealed both a higher exchange current density (i_0) and a lower activation energy for ORR. Therefore, this method can be used to improve the electrochemical performance of cathodes for SOFCs.

Acknowledgement

The authors would like to thank the National Science Council of Taiwan for financially supporting this research under Contract No. NSC 99-2113-M-259-003.

References

[1] B. Zhu, X. Liu, Z. Zhu, R. Ljungberg, Solid oxide fuel cell (SOFC) using industrial grade mixed rare-earth oxide electrolytes, Int. J. Hydrogen Energy 33 (2008) 3385–3392.

[2] H. Gu, H. Chen, L. Gao, Y. Zheng, X. Zhu, L. Guo, Effect of Co doping on the properties of $Sr_{0.8}Ce_{0.2}MnO_{3-\delta}$ cathode for intermediate-temperature solid oxide fuel cells, Int. J. Hydrogen Energy 33 (2008) 4681–4688.

[3] Y. Guo, H. Shi, R. Ran, Z. Shao, Performance of $SrSc_{0.2}Co_{0.8}O_{3-\delta}$ + $Sm_{0.5}Sr_{0.5}CoO_{3-\delta}$ mixed-conducting composite electrodes for oxygen reduction at intermediate temperatures, Int. J. Hydrogen Energy 34 (2009) 9496–9504.

[4] H. Moon, S.D. Kim, S.H. Hyun, H.S. Kim, Development of IT-SOFC unit cells with anode-supported thin electrolytes via tape casting and co-firing, Int. J. Hydrogen Energy 33 (2008) 1758–1768.

[5] T. Horita, K. Yamaji, M. Ishikawa, N. Sakai, H. Yokokawa, T. Kawada, Actives sites imaging for oxygen reduction at $La_{0.9}Sr_{0.1}MnO_{3-x}$/yttria-stabilized zirconia interface by secondary-ion mass spectrometry, J. Electrochem. Soc. 145 (1998) A3196–A3202.

[6] P.N. Dyer, R.E. Richards, S.L. Russck, D.M. Taylor, Ion transport membrane technology for oxygen separation and syngas production, Solid State Ionics 134 (2000) 21–33.

[7] J.P.P. Huijsmans, F.P.F. Van Berkel, G.M. Christie, Intermediate temperature SOFC – a promise for the 21st century, J. Power Sources 71 (1998) 107–110.

[8] B.C.H. Steele, K.M. Hori, S. Uchino, Kinetic parameters influencing the performance of IT-SOFC composite electrodes, Solid State Ionics 135 (2000) 445–450.

[9] W. Zhou, Z. Shao, R. Ran, P. Zeng, H. Gu, W. Jin, N. Xu, $Ba_{0.5}Sr_{0.5}Co_{0.8}Fe_{0.2}O_{3-\delta}$ + $LaCoO_3$ composite cathode for $Sm_{0.2}Ce_{0.8}O_{1.9}$-electrolyte based intermediate-temperature solid-oxide fuel cells, J. Power Sources 168 (2007) 330–337.

[10] T. Ishihara, M. Honda, T. Shibayama, H. Minami, H. Nishiguchi, T. Takita, Intermediate temperature solid oxide fuel cells using a new $LaGaO_3$ based oxide ion conductor. Part 1. Doped $SmCoO_3$ as a new cathode material, J. Electrochem. Soc. 145 (1998) 3177–3183.

[11] Y. Matsuzaki, I. Yasuda, Electrochemical properties of reduced-temperature SOFCs with mixed ionic–electronic conductors in electrodes and/or interlayers, Solid State Ionics 152-153 (2002) 463–468.

[12] S.P. Simner, M. Anderson, J.F. Bonnett, J. Stevenson, Enhanced low temperature sintering of (Sr, Cu)-doped lanthanum ferrite SOFC cathodes, Solid State Ionics 175 (2004) 79–81.

[13] S.P. Simner, J.F. Bonnett, N.L. Canfield, K.D. Meinhardt, J.P. Shelton, V.L. Sprenkle, J.W. Stevenson, Development of lanthanum ferrite SOFC cathodes, J. Power Sources 113 (2003) 1–10.

[14] A. Barbucci, R. Bozzo, G. Cerisola, P. Costamagna, Characterisation of composite SOFC cathodes using electrochemical impedance spectroscopy. Analysis of Pt/YSZ and LSM/YSZ electrodes, Electrochim. Acta 47 (2002) 2183–2188.

[15] X.D. Zhu, K.N. Sun, N.Q. Zhang, X.B. Chen, L.J. Wu, D.C. Jia, Improved electrochemical performance of $SrCo_{0.8}Fe_{0.2}O_{3-\delta}$–$La_{0.45}Ce_{0.55}O_{2-\delta}$ composite cathodes for IT-SOFC, Electrochem. Commun. 9 (2007) 431–435.

[16] S. Sun, X. Zhu, Y. Yuan, Electrochemical properties of $La_{0.8}Sr_{0.2}FeO_{3-\delta}$–$La_{0.45}Ce_{0.55}O_{2-\delta}$ composite cathodes for intermediate temperature SOFC, J. Solid State Electrochem. 14 (2010) 2257–2260.

[17] Y.P. Fu, S.B. Wen, C.H. Lu, Preparation and characterization of samaria-doped ceria electrolyte materials for solid oxide fuel cells, J. Am. Ceram. Soc. 91 (2008) 127–131.

[18] S.B. Adler, B.T. Henderson, M.A. Wilson, D.M. Taylor, R.E. Richards, Reference electrode placement and seals in electrochemical oxygen generators, Solid State Ionics 134 (2000) 35–42.

[19] J. Winkler, P.V. Hendriksen, N. Bonanos, M. Mogensen, Geometric requirements of solid electrolyte cells with a reference electrode, J. Electrochem. Soc. 145 (1998) 1184–1192.

[20] S.H. Chan, X.J. Chen, K.A. Khor, Reliability and accuracy of measured overpotential in a three-electrode fuel cell system, J. Appl. Electrochem. 31 (2001) 1163–1170.

[21] C.R. Xia, W. Rauch, F.L. Chen, M.L. Liu, $Sm_{0.5}Sr_{0.5}CoO_3$ cathodes for low-temperature SOFCs, Solid State Ionics 149 (2002) 11–19.

[22] H.J. Hwang, J.W. Moon, J. Moon, M. Awano, Removal of nitric oxide (NO) by perovskite-type composite catalytic thick film, $La_{0.6}Sr_{0.4}Co_{0.2}Fe_{0.8}O_{3-\delta}$ and gadolinia-doped ceria electrolyte, $Gd_{0.2}Ce_{0.8}O_{2-\delta}$, J. Am. Ceram. Soc. 88 (2005) 79–84.

[23] H.J. Hwang, J.W. Moon, S. Lee, E.A. Lee, Electrochemical performance of LSCF-based composite cathodes for intermediate temperature SOFCs, J. Power Sources 145 (2005) 243–248.

[24] Y. Leng, S.H. Chan, Q. Liu, Development of LSCF–GDC composite cathodes for low-temperature solid oxide fuel cells with thin film GDC electrolyte, Int. J. Hydrogen Energy 33 (2008) 3808–3817.

[25] J.X. Zhu, D.F. Zhou, S.R. Guo, J.F. Ye, X.F. Hao, X.Q. Cao, J. Meng, Grain boundary conductivity of high purity neodymium-doped ceria nanosystem with and without the doping of molybdenum oxide, J. Power Sources 174 (2007) 114–123.

[26] W. Zhou, R. Ran, Z. Shao, R. Cai, W. Jin, N. Xu, J. Ahn, Electrochemical performance of silver-modified $Ba_{0.5}Sr_{0.5}Co_{0.8}$ $Fe_{0.2}O_{3-\delta}$ cathodes prepared via electrodes deposition, Electrochim. Acta 53 (2008) 4370–4380.

[27] S.B. Adler, Limitations of charge-transfer models for mixed-conducting oxygen electrodes, Solid State Ionics 135 (2000) 603–612.

[28] C. Fu, K. Sun, N. Zhang, X. Chen, D. Zhou, Electrochemical characteristics of LSCF–GDC composite cathodes for intermediate temperature SOFC, Electrochim. Acta 52 (2007) 4589–4594.

[29] F. Qiang, K.N. Sun, N.Q. Zhang, X.D. Zhu, S.R. Le, D.R. Zhou, Characterization of electrical properties of GDC doped A-site deficient LSCF based composite cathode using impedance spectroscopy, J. Power Sources 168 (2007) 338–345.

[30] S.B. Adler, Factors governing oxygen reduction in solid oxide fuel cell cathodes, Chem. Rev. 104 (2004) 4791–4843.

[31] M. Kleitz, F. Petitbon, Optimized SOFC electrode microstructure, Solid States Ionics 92 (1996) 65–74.

[32] A. Ringuede, J. Fouletier, Oxygen reaction on strontium-doped lanthanum cobaltite dense electrodes at intermediate temperatures, Solid States Ionics 139 (2001) 167–177.

[33] J. Piao, K. Sun, N. Zhang, X. Chen, S. Xu, D. Zhou, Preparation and characterization of $Pr_{1-x}Sr_xFeO_3$ cathode material for intermediate temperature solid oxide fuel cells, J. Power Sources 172 (2007) 633–640.

[34] J. Liu, A.C. Co, B. Paulson, V.I. Briss, Oxygen reduction at sol–gel derived $La_{0.8}Sr_{0.2}Co_{0.8}Fe_{0.2}O_3$ cathode, Solid State Ionics 177 (2006) 377–387.

[35] A.C. Co, S.J. Xia, V.I. Briss, A kinetic study of the oxygen reduction reaction at $LaSrMnO_3$–YSZ composite electrodes, J. Electrochem. Soc. 152 (2005) A570–A576.